

High Fidelity Simulations of Airborne Virus Inactivation in a UV Air Purifier: Impact of Volumetric Flow Rate and UV Radiation Intensity

S. Sankurantripati, F. Duchaine, N. Francois, and S. Marshall

1 Introduction

The COVID-19 pandemic, caused by the pathogen, Severe Acute Respiratory Syndrome Coronavirus-2 (SARS-CoV-2), emerged in 2019 and has spread globally. This virus is transmitted through three modes: surface/contact, droplet and airborne. Airborne transmission is recognized as the dominant route [1]. Basic preventive measures like social distancing, sanitation, and face masks have reduced infection spread through contact and droplet transmission. To mitigate infection risk due to the virus-laden droplets suspended in air, it is crucial to implement high-quality, scientifically peer-reviewed solutions. Ultraviolet Germicidal Irradiation (UVGI) stands as a proven and dependable technological solution for disinfecting microorganisms found in water or on surfaces. Introducing a portable UV air purifier (UVP) into an enclosed space represents a potential mitigation solution capable of enhancing air quality. In this study, disinfection properties of a UVP designed by VALEO to equip city buses are analyzed by numerical simulations. It is composed of axial fans, UV-C lamps, light traps and an electric tray as shown in Fig. 1. This research focuses on airborne virus inactivation using a multi-disciplinary solver, integrating Large Eddy Simulations (LES) for flow dynamics, Lagrangian particle tracking for airborne dispersion and a UV radiation disinfection solver for assessing survival rates. The study explores varying purifier flow rates and UV lamp power to observe survival rates of virus copies.

S. Sankurantripati · F. Duchaine
CFD department, CERFACS, e-mail: sankurantripati@cerfacs.fr

N. Francois · S. Marshall
VALEO, e-mail: nicolas-yoan.francois@valeo.com

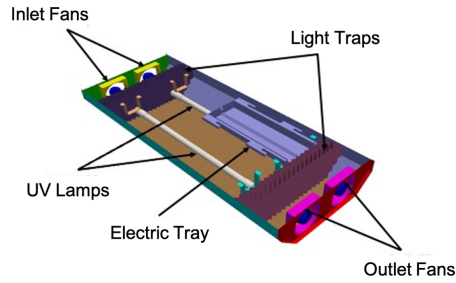


Fig. 1: View of UV air purifier designed by VALEO.

2 Computational Methodology

Studying the survival rates of respiratory droplets inside a UV radiation-exposed air purifier involved extensive high-fidelity computations over seconds to minutes, consuming millions of computational hours. First, airflow inside the UVP is calculated until the volume-averaged kinetic energy stabilizes. Since aerosols minimally impact the flow field, the resulting mean flow and turbulence characteristics are used for Lagrangian computations, where the air flow remains constant, and only particle dynamics are calculated [2]. This Eulerian-Lagrangian approach is coupled with UV radiation and disinfection models to determine inactivation of virus-laden droplets.

The AVBP LES solver from CERFACS [3] is used to solve the filtered compressible Navier-Stokes equations, utilizing the Lax-Wendroff scheme [4] for convection terms and a second-order Galerkin scheme for diffusion. Simulations depend on the CFL number, set to 0.9. The WALE model is used for sub-grid scale viscosity. Each respiratory droplet is modeled as a rigid sphere containing water, non-volatile matter, and virus copies, with interactions among particles disregarded and wall collisions considered inelastic. Virus copy distribution per droplet is modeled from experimental data on sneezing and coughing [5]. The Abramzon-Sirignano model calculates droplet evaporation, and once evaporated, the remaining solid matter is treated as a spherical droplet nucleus. Flow properties are interpolated to droplet locations to compute forces, simplified to momentum transfer via drag forces, ignoring gravity. A Langevin model [6, 2] includes turbulent quantities in the Lagrangian calculations.

The inactivation rate (S) of virus-laden droplets when exposed to UV radiation for a given exposure time can be calculated using the Chick-Watson model [7], as shown in Eq. 1. Here, k is the susceptibility constant of the virus, which depends on the UV wavelength used for inactivation and the medium of exposure, and varies for each virus. For SARS-CoV-2, susceptibility constant in air medium is not available. Therefore, a decent estimate based on available data on airborne viruses [8], is considered for this current study ($k = 0.377 \pm 0.119 m^2/J$). I represents the UV irradiance received by particles from a cylindrical UV lamp, determined using a

thermal radiation view-factor model [9]. The cumulative UV radiation received by each droplet inside the purifier is computed until it exits through the outlet fans.

$$S(t_e) = 1 - e^{kt_e}; \quad (1)$$

An unstructured mesh comprising 49 million cells is used for computational investigations following mesh convergence studies. Three cases with volumetric flow rates (VFR) of 75, 100, and 150 m^3/hr are simulated by enforcing a constant mass flow rate at the inlet fans, maintaining a uniform temperature of 300 K, and setting pressure outlets at the outlet fans to 1 *atm*. A body force approach is used to mimic swirl motion generated by axial fans. To take into account the temperature effects, UV lamps are considered isothermal and no-slip conditions with a reference temperature of $T_{lamp} = 311$ K. The remaining walls are provided adiabatic, no-slip wall conditions. To mimic aerosols, injected particle size is assumed mono-disperse with a diameter of $50\mu m$ and viral load concentration of 2.35×10^9 virus copies/*ml*. Impact of UV lamp output power (W_l) on survival rate of virus copies is evaluated by changing $W_l = W_o, W_o/1.5, W_o/2, W_o/3, W_o/4$ and $W_o/6$ where $W_o = 13W$ for $k = 0.258, 0.377$ and $0.496 m^2/J$. It is important to note that droplet injection rate remains same for all these above-mentioned simulation setups.

3 Results and Discussion

3.1 Eulerian Phase

Large eddy simulations of the UVP were conducted on the Irene-Rome supercomputers hosted by TTGC (GENCI, allocation number: A0142A06074) for 6 convection cycles, requiring around 768,000 computational hours for flow field convergence and extraction of mean and turbulent quantities. The time-averaged velocity distribution inside the purifier, normalized by the velocity near the inlet fans, is shown in Figure 2, along with an iso-contour of axial velocity ($u = 0$). Air entering through the inlet fans undergoes a swirling motion, creating a hollow disk-like stream profile with high transverse and axial velocities. A recirculation zone is observed between the inlet light traps and fans, resulting from the strong swirling motion. Light traps streamline airflow towards the tray side, creating a recirculation zone on the opposite side, as shown by iso-lines of axial velocity. Turbulent activity inside the UVP is depicted in Figure 3 using time-averaged turbulent kinetic energy contours. Interactions between hollow-shaped flow motion and recirculation regions cause high levels of turbulence, which intensifies as the turbulent flow enters light traps, collides with walls, and mixes. Pockets of turbulent activity are detected near the electric tray due to streamlined flow impact and dispersion. Turbulence is also detected at the outlet fans and light traps, stronger on the side opposite the electric tray, caused by mixing from recirculation regions and dispersed flow. As the volumetric flow rate (VFR) increases from 75 to 150 m^3/hr , both turbulent kinetic

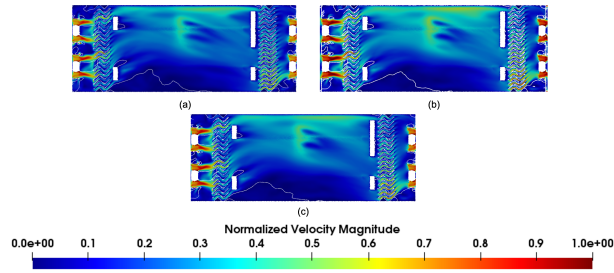


Fig. 2: Time-averaged velocity magnitude profiles inside the purifier normalized to velocity near inlet fans ($v_{norm} =$ (a) 3.8m/s, (b) 5.067 m/s, (c) 7.2m/s) along with an iso-contour ($u=0$) for 3 volumetric flow rates (VFR): (a) $75 \text{ m}^3/\text{hr}$, (b) $100 \text{ m}^3/\text{hr}$, (c) $150 \text{ m}^3/\text{hr}$.

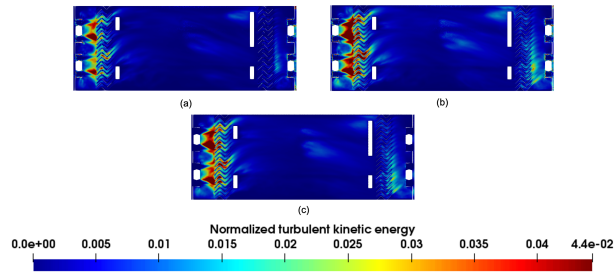


Fig. 3: Time-averaged turbulent kinetic energy contours inside the purifier normalized to squared velocity near inlet fans ($v_{norm} =$ (a) 3.8m/s, (b) 5.067 m/s, (c) 7.2m/s) for 3 volumetric flow rates (VFR): (a) $75 \text{ m}^3/\text{hr}$, (b) $100 \text{ m}^3/\text{hr}$, (c) $150 \text{ m}^3/\text{hr}$.

energy and velocity flow fields rise, although the flow patterns remain similar across different VFRs. In summary, light traps, inlet fans, and the electric tray significantly shape the flow inside the UVP, creating large recirculation regions, high turbulence, and strong mixing. Increasing VFR intensifies turbulent activity and velocities without altering the flow pattern. The impact of these flow fields on virus-laden droplets is discussed in the next section.

3.2 Lagrangian Phase

Virus-laden droplets are introduced into a purifier at the inlet fans and collected at the outlet fans. Using Lagrangian tracking, the movement of these particles is monitored until their number stabilizes as shown in Fig. 5. This simulation, which took 19,500 computational hours for a 30-second physical duration, revealed that at a volumetric flow rate (VFR) of $75 \text{ m}^3/\text{hr}$, particle accumulation is higher compared to higher VFRs ($100 \text{ m}^3/\text{hr}$ and $150 \text{ m}^3/\text{hr}$) due to velocity differences. Figure 4

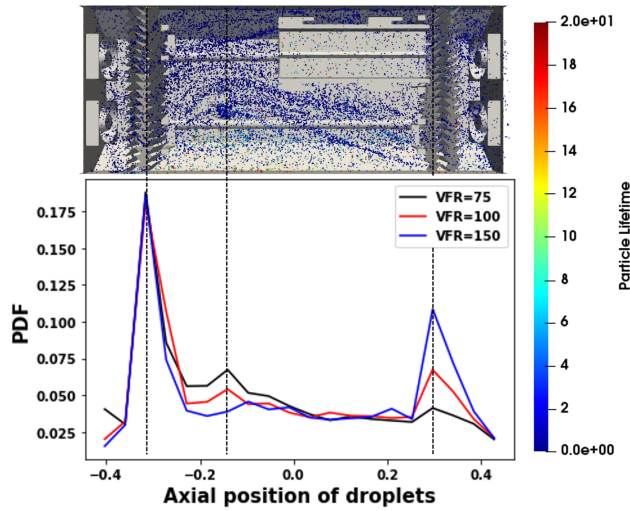


Fig. 4: Instantaneous snapshot of particle dispersion colored with particle lifetime inside the UVP and PDF of axial location of particles for 3 volumetric flow rates at time = 25s.

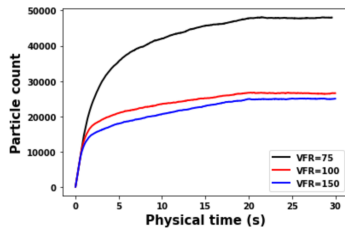


Fig. 5 Convergence of number of particles inside purifier with time for 3 volumetric flow rates (VFR)

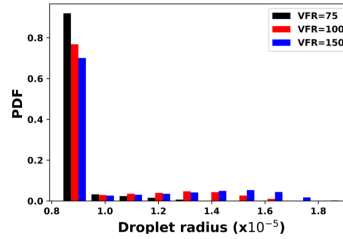


Fig. 6 PDF of droplet radius collected at the exit of the purifier over a 5-second interval for three volumetric flow rates.

shows the axial distribution of particles, with most being new and having lifetimes under 4 seconds. Particles with longer lifetimes are found near the inlet and outlet light traps, the electric tray, and the large recirculation zone. The probability density function (PDF) indicates three peaks of high particle accumulation: the highest at the inlet light trap, the second highest at the outlet light trap, and the last at the large recirculation zone.

Figures 6 and 7 illustrate the droplet radius and residence time of UV-radiation-treated particles collected at the outlet over a 5-second interval. These figures indicate that the majority of the exited particles are droplet nuclei exposed to radiation for a maximum of 0.6 seconds. Comparing these histograms reveals that the volumetric flow rate determines the size and residence time of the expelled particles. As VFR increases, residence time of droplets inside the purifier reduces, resulting

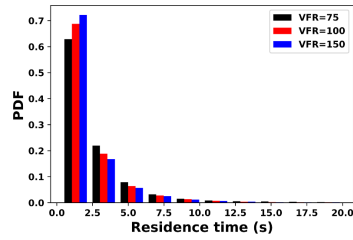


Fig. 7 PDF of residence time collected at the exit of the purifier over a 5-second interval for three volumetric flow rates.

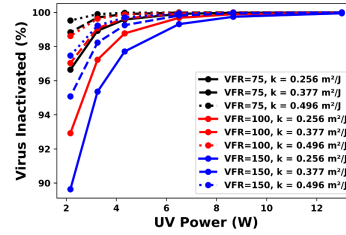


Fig. 8 Overall Inactivation rate of this UVP in an interval of 5s by varying UV lamp power output and volumetric flow rate

in a lower overall inactivation rate. Figure 8 shows the virus inactivation rate over a 5-second interval achieved by the UVP under various UV radiation intensities. A decrease in UV lamp power (W_l) from the original power (W_o) to one-sixth of it ($W_o/6$) leads to an exponential reduction in the inactivation rate. The susceptibility constant also significantly impacts the resulting inactivation rate.

This parametric study reveals that higher mass flow rates enable the purifier to treat a larger volume of air in less time while still achieving a virus inactivation rate of 95% by exposing all the virus-laden droplets to UV radiation.

References

1. R. Zhang, Y. Li, A. L. Zhang, Y. Wang, M. J. Molina, *Identifying airborne transmission as the dominant route for the spread of COVID-19*, *The COVID-19 Reader*, 2020, pp. 21–35, doi: 10.4324/9781003141402-3
2. F. Duchaine, M. Cizeron, N. Odier, J. Dombard, S. Marshall, N. Francois, T. Poinot, *High-performance CFD for respiratory droplet turbulent dispersion in a ventilated city bus*, *International Journal of Computational Fluid Dynamics*, 2021, **35**(9), pp. 758–777, doi: 10.1080/10618562.2021.1989421
3. T. Schonfeld, M. Rudgyard, *Steady and unsteady flow simulations using the hybrid flow solver AVBP*, *AIAA Journal*, 1999, **37**(11), pp. 1378–1385, doi: 10.2514/2.636
4. P. D. Lax, B. Wendroff, *Difference schemes for hyperbolic equations with high order of accuracy*, *Communications on pure and applied mathematics*, 1964, **17**(3), pp. 381–398, publisher: Wiley Online Library
5. S. Anand, Y. S. Mayya, *Size distribution of virus-laden droplets from expiratory ejecta of infected subjects*, *Scientific reports*, 2020, **10**(1), p. 21174, publisher: Nature Publishing Group UK London
6. P. Langevin, *Sur la théorie du mouvement brownien*, *C. R. Acad. Sci. Paris.*, 1908, **146**, pp. 530–533.
7. H. Chick, *An investigation of the laws of disinfection*, *Journal of Hygiene*, 1908, **8**(1), pp. 92–158, doi: 10.1017/s0022172400006987
8. C. B. Beggs, E. J. Avital, *Upper-room ultraviolet air disinfection might help to reduce COVID-19 transmission in buildings: A feasibility study*, *PeerJ*, 2020, **8**, doi: 10.7717/peerj.10196
9. M. F. Modest, S. Mazumder, *Radiative heat transfer*, 2021, publisher: Academic Press